Inorganic Chemistry

ARTICLE

pubs.acs.org/IC

Pyridazine- versus Pyridine-Based Tridentate Ligands in First-Row Transition Metal Complexes

Katrin R. Grünwald,[†] Manuel Volpe,[†] Pawel Cias,[‡] Georg Gescheidt,[‡] and Nadia C. Mösch-Zanetti*[,†]

[†]Institut für Chemie, Bereich Anorganische Chemie, Karl-Franzens Universität Graz, Schubertstrasse 1, A-8010 Graz, Austria

[‡]Institut für Physikalische und Theoretische Chemie, Technische Universität Graz, Stremayrgasse 9/I (A), A-8010 Graz, Austria

Supporting Information

ABSTRACT:

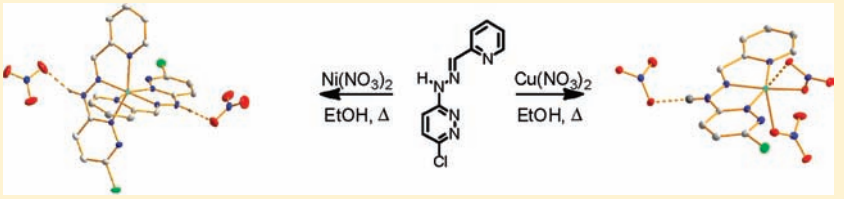

A series of first-row transition metal complexes with the unsymmetrically disubstituted pyridazine ligand picolinaldehyde (6-chloro-3-pyridazinyl)hydrazone (PIPYH), featuring an easily abstractable proton in the backbone, was prepared. Ligand design was inspired by literature-known picolinaldehyde 2-pyridylhydrazone (PAPYH). Reaction of PIPYH with divalent nickel, copper, and zinc nitrates in ethanol led to complexes of the type $[Cu^{II}(PIPYH)(NO_3)_2]$ (**1**) or $[M(PIPYH)_2](NO_3)_2$ [M = Ni^{II} (**2**) or Zn^{II} (**3**)]. Complex synthesis in the presence of triethylamine yielded fully- or semideprotonated complexes $[Cu^{II}(PIPY)(NO_3)]$ (**4**), $[Ni^{II}(PIPYH)(PIPY)](NO_3)$ (**5**), and $[Zn^{II}(PIPY)_2]$ (**6**), respectively. Cobalt(II) nitrate is quantitatively oxidized under the reaction conditions to $[Co^{III}(PIPY)_2](NO_3)$ (**7**) in both neutral and basic media. X-ray diffraction analyses reveal a penta- (**1**) or hexa-coordinated (**2**, **3**, and **7**) metal center surrounded by one or two tridentate ligands and, eventually, κ-O,O′ nitrate ions. The solid-state stoichiometry was confirmed by electron impact (EI) and electrospray ionization (ESI) mass spectrometry. The diamagnetic complexes **5** and **6** were subjected to ^{1}H NMR spectroscopy, suggesting that the ligand to metal ratio remains constant in solution. Electronic properties were analyzed by means of cyclic voltammetry and, in case of copper complexes **1** and **4**, also by electron paramagnetic resonance (EPR) spectroscopy, showing increased symmetry upon deprotonation for the latter, which is in accordance with the proposed stoichiometry $[Cu^{II}(PIPY)(NO_3)]$. Protic behavior of the nickel complexes **2** and **5** was investigated by UV/vis spectroscopy, revealing high π-backbonding ability of the PIPYH ligand resulting in an unexpected low acidity of the hydrazone proton in nickel complex **2**.

INTRODUCTION

Pyridazines find wide application in drug design[1−3] and as potential fungicides,[4−6] explaining the development of numerous organic derivatives. In contrast, coordination chemistry of pyridazines is limited, especially compared to related chemistry of pyridines. The second nitrogen atom in the heterocyclic system leads on one hand to a more electron-deficient ring system with limited σ-donating abilities, which is reflected by the acid constants (pK_a 2.24 for parent pyridazine vs pK_a 5.25 for pyridine), whereas on the other hand effective π-backbonding is enabled by significantly lowered molecular orbitals. Due to the different electronic situation in comparison to pyridine systems, unique chemical behavior can be expected. Pyridazine offers in principle the possibility to coordinate two metal atoms in close proximity. However, such behavior is observed only in pyridazine ligands with preformed compartments or in macrocyclic systems.[7−14] In order to accommodate two metals, the pyridazine ring needs to be substituted in 3- and 6-positions with two donors to exploit the chelate effect and thus increase the binding tendency of the electron-poor second nitrogen donor. Simple complexes without additional donors or secondary bridging functionalities featuring pyridazine as a terminal ligand[15] display significantly different electronic ligand properties in comparison to pyridine.

Suitable synthetic pathways are available for symmetric substitution of 3,6-diformylpyridazine.[13] Pyridazines with only one additional donor next to a ring-nitrogen atom leading to bi- or tridentate ligands are synthetically more challenging and thus have been significantly less investigated in coordination chemistry.[16−19]

We have recently described an easy entry into pyridazine chemistry with a methylhydrazone pyridyl substituent next to one of the nitrogen atoms (picolinaldehyde 3-pyridazinyl-*N*-methylhydrazone, PIPYMe), with which coordination chemistry of first-row transition metals was explored.[20] Here, the preparation of an unsubstituted hydrazone ligand [picolinaldehyde (6-chloro-3-

Received: February 9, 2011
Published: July 15, 2011

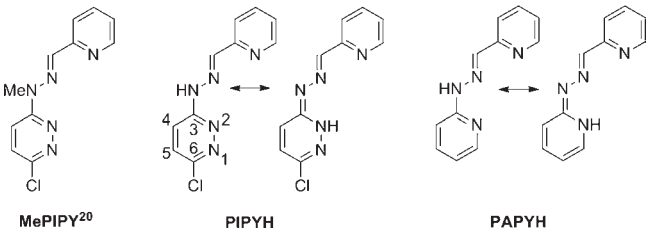

Figure 1. Ligand system presented in this work in comparison to the parent PAPYH system.

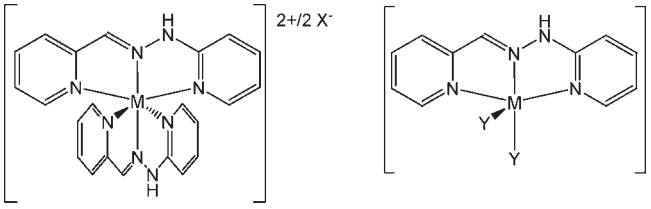

Figure 2. Complexes containing PAPYH with two different metal to ligand ratios.

pyridazinyl)hydrazone, PIPYH] is described, which is reminiscent of the existing picolinaldehyde 2-pyridylhydrazone (PAPYH) system (Figure 1), allowing direct comparison of a pyridine- and a pyridazine-based system. Both PIPYH and PAPYH feature a tautomerizable proton in contrast to the methyl derivative PIPYMe, which may give rise to interesting properties and applications.

PAPYH, first reported in 1957,[21] is a powerful chelating ligand coordinating in a meridional tridentate mode similar to terpyridine.[22−26] In contrast, it features a significantly more flexible hydrazone bridge and a secondary amine functionality with a proton in the ligand backbone whose pronounced acidity increases upon coordination.[22,27,28] Thus, it can be easily removed with a base and readded with an acid, reversibly. The deprotonated complexes are readily soluble in a variety of organic solvents and were found to be intensely colored, rendering them suitable acid−base indicators.[28,29] Due to their extraordinary stability toward acids and bases, apart from de- or reprotonation, $PAPYH/PAPY^-$ solutions allow for selective extraction of various metals from aqueous media.[30,31]

Coordination chemistry of PAPYH has been thoroughly investigated. The tridentate ligand coordinates strongly to divalent metal ions, forming octahedral complexes of the type $[M(PAPYH)_2]X_2$ (e.g., X = ClO_4^- or PF_6^-) or square pyramidal complexes containing only one PAPYH molecule $[M(PAPYH)Y_2]$ (e.g., Y = Br or Cl) depending on the counterion (Figure 2).[24,27]

Among late first-row transition metals, cobalt(II) salts behave differently. Due to the relative instability of the divalent state, Co^{II} is readily oxidized to Co^{III} by PAPYH, presumably under formation of molecular hydrogen.[32] The resulting semiprotonated 2:1 complex $[Co^{III}(PAPYH)(PAPY)]^{2+}$ is readily fully deprotonated, for example, by recrystallization from aqueous ethanol.[23]

The deprotonated $PAPY^-$ anion is fully aromatic, which leads to a distribution of the formal charge at the hydrazone nitrogen all over the molecule. Detailed studies on the location of the charge in the PAPYH system or in related frameworks have not been reported yet.

Scheme 1. Synthesis of Ligand PIPYH[a]

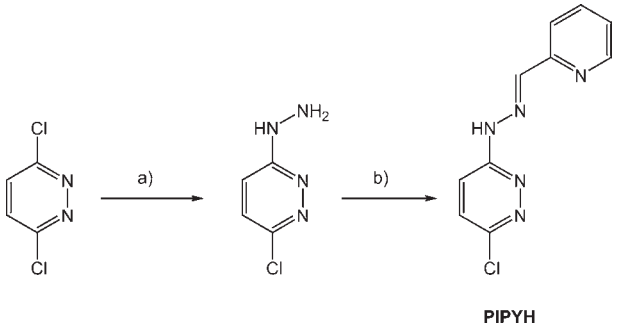

[a] (a) Hydrazine (1.6 equiv) in water/NH_3, reflux, 3 h.[33] (b) 2-Pyridinecarbaldehyde (1.1 equiv) in EtOH (3 drops of acetic acid), reflux, 2 h.

Here, the syntheses of a series of PIPYH complexes with the first-row transition metals cobalt, nickel, copper, and zinc are described. Investigations of their protic behavior, their structural properties by single-crystal X-ray diffraction analyses, and their electronic properties by cyclic voltammetry and by electron spin resonance spectroscopy are compared to the behavior of the PAPY pyridyl system, revealing interesting differences.

RESULTS AND DISCUSSION

Synthesis of Ligand. Ligand PIPYH was synthesized in a two-step procedure as shown in Scheme 1. Substitution of one chlorine of 3,6-dichloropyridazine with hydrazine proceeded smoothly in boiling aqueous ammonia, yielding a white product in high purity. Monosubstitution was evidenced by ^1H NMR spectroscopy, as the singlet assignable to the equivalent aromatic protons of the starting material at 7.51 ppm splits into two doublets at 7.26 and 7.13 ppm. Two broad signals at 6.62 and 2.78 ppm in the ratio of 1:2 for one secondary NH and two primary NH_2 protons appear in the spectrum. Subsequent Schiff-base condensation employing 2-pyridinecarbaldehyde in ethanol gave the ligand in the form of white needles. Imine formation is evidenced by a new singlet at 8.16 ppm in the ^1H NMR spectrum. Two shifted pyridazine doublets at 7.76 and 7.71 ppm and the shifted broad resonance at 11.97 ppm for the acidic N*H* proton indicate quantitative formation of PIPYH.

Synthesis of Complexes. The coordinating ability of PIPYH toward the first-row transition metals nickel, copper, and zinc was investigated. Addition of an ethanol solution of the respective metal salt $[Ni(NO_3)_2 \cdot 6H_2O$, $Cu(NO_3)_2 \cdot 3H_2O$, or $Zn(NO_3)_2 \cdot 4H_2O]$ to a boiling ethanol solution of PIPYH led in all cases to an immediate color change from pale yellow to brown. After cooling to room temperature and slow evaporation of the solvent in all three reaction solutions, crystals suitable for X-ray diffraction analysis were obtained. For copper, determination of the molecular structure revealed the formation of complex $[Cu^{II}(PIPYH)(NO_3)_2]$ (**1**) with 1 equiv of the hydrazone ligand and two coordinated nitrate ligands. The direct inlet electron impact mass spectrometry (EI-MS) spectrum of solid **1** shows $[Cu(PIPY)(NO_3)]^+$. This is consistent with the literature, where copper complexes of 1:1 stoichiometry are also reported for PAPYH, especially when coordinating counterions are present.[24,25] However, titration studies of the PAPY complexes showed that, in solution, various complexes with different metal to ligand ratios are present.[32] In agreement with that, the

dx.doi.org/10.1021/ic200279g |*Inorg. Chem.* 2011, 50, 7478–7488

Scheme 2. Formation of Complexes 1−6 Employing Neutral PIPYH or Monoanionic PIPY⁻

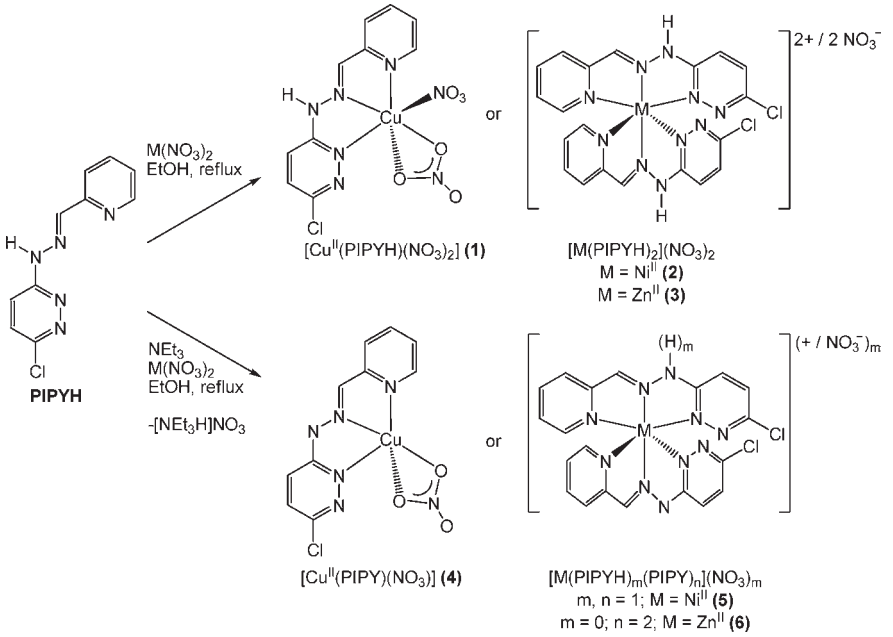

electrospray ionization mass spectometry (ESI-MS) spectrum of **1** in acetonitrile seems to show the presence of several species.

In the case of nickel and zinc, dicationic complexes of the type $[M(PIPYH)_2](NO_3)_2$ [M = Ni^{II} (**2**) or Zn^{II} (**3**)] were formed regardless of the employed stoichiometry (Scheme 2). This was further confirmed by direct inlet EI-MS analyses of solid samples of **2** and **3**. Solution ESI mass spectrometry of complex **2** shows the $[M(PIPYH)_2 - H]^+$ peak as well. All complexes feature tridentate ligand molecules, which coordinate in a meridional fashion. Although the complexes possess low solubility in common organic solvents, the concentration was enough for recording CV data. In the case of zinc complex **3**, dissolution in CD_3CN caused decomposition of the complex, evidenced by the appearance of free ligand signals in the ^1H NMR spectrum.

Deprotonated Complexes. Addition of PIPYH to the metal nitrate solution in the presence of 1 equiv of triethylamine led, in the case of copper and nickel nitrate, to intensely colored crystalline precipitates (Scheme 2). With copper, we believe that the deprotonated complex $[Cu^{II}(PIPY)(NO_3)]$ (**4**) was formed, as evidenced by elemental analysis. Direct inlet EI-MS of the solid sample shows the molecular ion $[Cu(PIPY)]^+$ with the correct isotopic pattern, whereas a peak for $[Cu(PIPY)_2]^+$ is consistently absent, identical to the data found for **1**. According to ESI-MS in acetonitrile, again, several species seem to be present in solution, in agreement with the behavior seen for related PAPY complexes.[32] In both cases, mass spectrometry is unsuitable to distinguish between compounds of types $[Cu(LH)(NO_3)_2]$ and $[Cu(L)(NO_3)]$. For this reason, compounds **1** and **4** were further investigated by electron paramagnetic resonance (EPR) spectroscopy supporting their formulation (vide infra).

With nickel, the semideprotonated compound $[Ni^{II}(PIPYH)(PIPY)](NO_3)$ (**5**) is presumably formed. Also, the two nickel complexes **2** and **5** show identical solid-state EI-MS data, the molecular ion being $[Ni(PIPYH)(PIPY)]^+$. In contrast to the copper complexes **1** and **4**, complex **5** seems more stable toward ligand substitution as the ESI mass spectrum in acetonitrile also shows the highest mass to be $[Ni(PIPYH)(PIPY)]^+$. This indicates identical L:M = 2:1 ratios for both complexes. Furthermore, the absence of a molecular ion for $[Ni(PIPY)_2]^+$, together with the elemental analysis data, points to the formation of a semideprotonated compound rather than $[Ni(PIPY)_2]$.

The reaction of zinc nitrate with a mixture of PIPYH and NEt_3 in ethanol yielded a yellow clear solution after cooling to room temperature. Evaporation of the solvent gave a yellow suspension, from which a waxy solid was isolated by centrifugation and washed with diethyl ether. The material is well soluble in ethanol but only slightly in acetonitrile. For reasons of comparison, a ^1H NMR spectrum was recorded in CD_3CN, although an overnight measurement was necessary (Figure 3). It shows one set of resonances assignable to the protons of the deprotonated ligand due to the absence of an N−H resonance. All aromatic signals are significantly shifted compared to those of PIPYH. For this reason, we believe that the symmetric doubly deprotonated complex $[Zn(PIPY)_2]$ (**6**) is formed. Furthermore, EI-MS shows a peak with the expected isotopic pattern for $[Zn(PIPY)_2]^+$. The upfield shift of the aromatic resonances is presumably due to a certain degree of metal-to-ligand π-backbonding.

Reactivity toward a Cobalt(II) Salt. The reaction of $Co(NO_3)_2 \cdot 6H_2O$ with 1 equiv of PIPYH in the presence as well as in absence of triethylamine led to isolation of the same product (Scheme 3), in contrast to the above-described behavior. The ligand solution in boiling ethanol with or without triethylamine turned immediately deep purple upon addition of the metal salt solution. After cooling to room temperature, a brown solid was formed upon removal of the solvent. When this material was recrystallized from ethanol, small dark green single crystals started to grow as the solvent slowly evaporated overnight. Redissolution of these crystals in polar solvents such as dimethyl sulfoxide (DMSO), acetonitrile, methanol, or ethanol reinstated the intensively purple-colored solution. The obtained crystals proved to be suitable for X-ray diffraction analysis, which revealed the formation of complex $[Co^{III}(PIPY)_2](NO_3)$ (**7**) with two coordinated hydrazone ligands and 1.5 molecules of ethanol in the unit cell. The presence of the latter probably

dx.doi.org/10.1021/ic200279g |*Inorg. Chem.* 2011, 50, 7478–7488

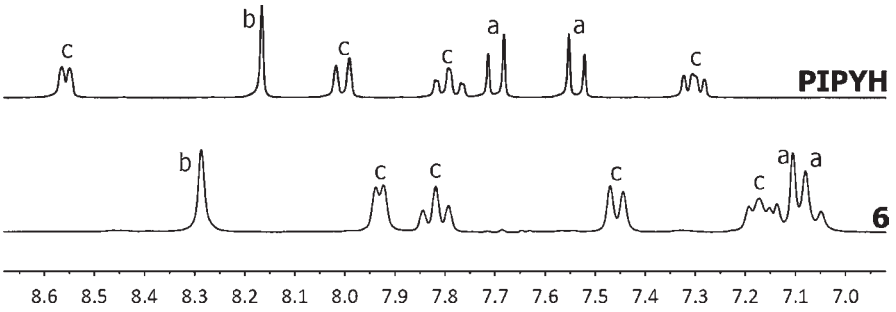

Figure 3. ^{1}H NMR spectra (aromatic region in CD_3CN) of ligand PIPYH and complex $[Zn(PIPY)_2]$ (**6**): (a) pyridazine, (b) imine, and (c) pyridyl proton resonances.

Scheme 3. Formation of Cobalt Complex 7 Employing PIPYH in the Presence and Absence of NEt_3

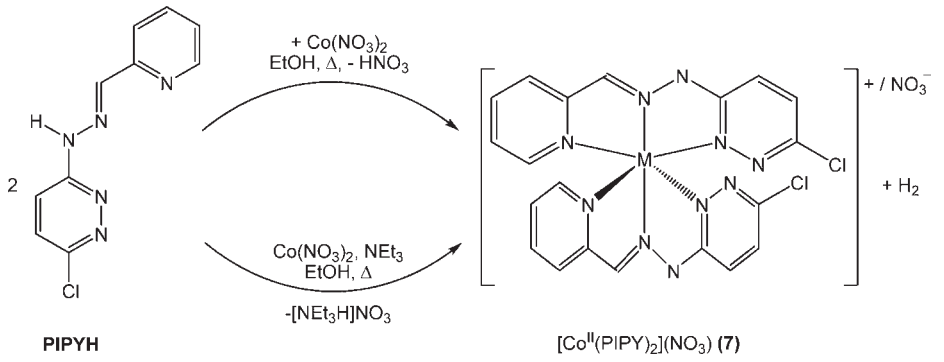

justifies the different color of the crystals compared to the isolated compound, a brown amorphous powder. One nitrate counterion was found in the unit cell, pointing to the oxidation of Co^{II} to Co^{III}. This fact is further supported by the Co−N bond distances, which fall in the range reported for Co^{III}−N, whereas significantly longer distances would be expected in the case of the divalent state.[34] In the ^{1}H NMR spectrum, complex **7** exhibits sharp resonances in CD_3CN as expected for the Co^{III} d^6 low-spin center. ^{1}H NMR spectra of the purple acetonitrile solutions of the brown material and the green crystals are identical and show one set of signals for a coordinated $PIPY^-$ ligand. In the spectrum of the green crystals, ethanol was found, which integrates for 1.5 molecules per cobalt. Due to poor solubility of the complex, no ^{13}C NMR spectra could be obtained even after prolonged measurement. Elemental analysis of both materials confirms the composition and points to identical complexes. Furthermore, EI mass spectrometry shows the formation of the $[Co(PIPY)_2]^+$ core for both materials. Deprotonated $PAPY^-$ complexes show high solubilities in organic solvents including benzene and chloroform,[27] which is why they have been proposed for ion extraction applications from water.[30,31] In contrast to that, the solubility of cobalt complex **7** is dramatically decreased, with it being soluble only in polar solvents such as ethanol or acetonitrile and completely insoluble in tetrahydrofuran (THF) or ethers.

Similar to the behavior of PAPYH, the cobalt ion in **7** is presumably oxidized by the PIPYH ligand, consistent with oxidizing ability of PAPYH solutions toward Co^{II} ions, which was reported early on.[21,32] When the reaction was performed with rigorously degassed solvent under an Ar atmosphere, the identical diamagnetic compound was isolated in comparable

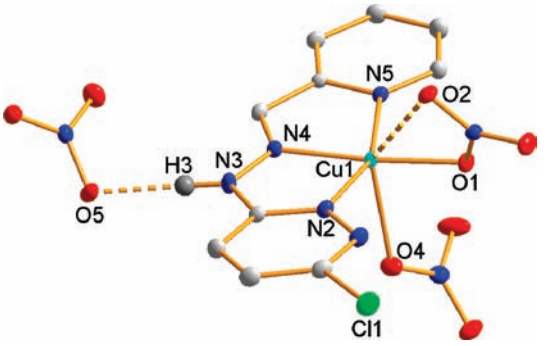

Figure 4. Molecular view of complex $[Cu^{II}(PIPYH)(NO_3)_2]$ (**1**) including a hydrogen-bonded nitrate ion of the neighboring complex ion (50% probability). Hydrogen atoms (except the hydrazone proton in the ligand backbone) have been omitted for clarity.

yields (64% based on the ligand). Layering an ethanol solution with dry and degassed diethyl ether in an argon atmosphere afforded green single crystals that proved to exhibit identical crystallographic parameters to those of crystals obtained under ambient conditions. Thus, oxygen can be excluded as the oxidizing agent and the ligand seems more likely to provide the redox equivalents by forming hydrogen. Furthermore, the reduction potential of $Co^{III} \rightarrow Co^{II}$ (−0.866 V vs Ag/Ag^+ or −0.621 V vs normal hydrogen electrode, NHE) points toward a spontaneous oxidation of the metal in the presence of protons.

Molecular Structures of Complexes. For all protonated complexes **1**−**3** as well as for complex **7**, single crystals suitable for crystallographic analyses could be obtained by slow evaporation of

dx.doi.org/10.1021/ic200279g |*Inorg. Chem.* 2011, 50, 7478–7488

Table 1. Selected Bond Lengths for Complexes 1−3 and 7

	bond length, Å			
bond	**1**	**2**[a]	**3**	**7**[b]
M−N2	2.0017(9)	2.1037(17)	2.1803(11)	1.901(7)
M−N4	1.9578(10)	2.0027(17)	2.0992(11)	1.875(8)
M−N5	1.9958(9)	2.1177(17)	2.2247(11)	1.948(7)
M−O1	1.9458(8)			
M−O4	2.2731(9)			
M−N7		2.1037(17)	2.1493(11)	1.904(7)
M−N9		2.0027(17)	2.1533(11)	1.876(8)
M−N10		2.1177(17)	2.1333(11)	1.937(8)

[a] Second ligand molecule generated by symmetry operation {#1 ($-x+2$, y, $-z+{}^{1}/_{2}$); #2 ($-x+2$, y, $-z+{}^{3}/_{2}$}: N2^{i}, N4^{i}, and N5^{i} are represented by N7, N9, and N10. [b] Data for only one molecule of the two found in the asymmetric unit are given.

Table 2. Selected Angles for Complexes 1−3 and 7

	bond angle, deg			
angle	**1**	**2**[a]	**3**	**7**[b]
N2−M−N4	78.99(4)	76.60(6)	73.44(4)	81.0(3)
N2−M−N5	157.61(4)	154.30(6)	147.44(4)	164.3(3)
N2−M−N7		96.58(9)	94.30(4)	91.1(3)
N2−M−N9		102.80(7)	121.47(4)	94.7(3)
N2−M−N10		91.26(7)	90.74(4)	91.1(3)
N4−M−N5	80.14(4)	77.81(7)	74.33(4)	83.3(3)
N4−M−N7		102.80(7)	102.78(4)	99.9(3)
N4−M−N9		179.12(10)	164.22(4)	175.8(3)
N4−M−N10		102.82(7)	112.82(4)	96.3(3)
N2−M−O1	100.81(4)			
N2−M−O4	85.05(4)			
N4−M−O1	174.59(4)			
N4−M−O4	100.10(4)			
N5−M−O1	99.19(4)			
N5−M−O4	106.60(4)			
O1−M−O4	85.24(4)			
N5−M−N7		91.26(7)	97.13(4)	90.2(3)
N5−M−N9		102.82(7)	91.06(4)	100.9(3)
N5−M−N10		92.17(9)	97.51(4)	92.0(3)
N7−M−N9		76.60(6)	72.63(4)	80.4(3)
N7−M−N10		154.30(6)	143.98(4)	163.8(3)
N9−M−N10		77.81(7)	74.37(4)	83.4(3)

[a] Second ligand molecule generated by symmetry operation {#1 ($-x+2$, y, $-z+{}^{1}/_{2}$); #2 ($-x+2$, y, $-z+{}^{3}/_{2}$}: N2^{i}, N4^{i}, and N5^{i} are represented by N7, N9, and N10. [b] Data for only one molecule of the two found in the asymmetric unit are given.

the solvent. Molecular views of complexes **1**, **2** and **7** are displayed in Figures 4−6. A representation of complex **3** is included in the Supporting Information (Figure S1). Selected bond lengths and angles are given in Tables 1 and 2, and crystallographic data are listed in Table 3.

In the copper complex [Cu^{II}(PIPYH)(NO$_3$)$_2$] (**1**) (Figure 4), the metal atom is coordinated by one neutral ligand and two nitrate ions to form a distorted square pyramidal geometry. The PIPYH ligand molecule is coordinated in a tridentate meridional mode to occupy three positions of the basal plane. The fourth corner and the apical position are taken by the oxygen atoms of two nitrates, which coordinate as terminal κ^1-O ligands. Similar square pyramidal configurations have previously been observed for copper halide complexes bearing also one PAPYH ligand.[24,25] O2 is approaching the second apical position of an octahedron, but the long atom distance [2.734(9) Å] implies only a weak interaction. The Cu1−N4 bond is the shortest metal−ligand distance [1.9578(10) Å] and is significantly shorter than Cu1−N2 and Cu1−N5, which are 2.0017(9) and 1.9958(9) Å, respectively, which is in perfect agreement with literature data of PAPYH copper(II) complexes.[24,25] The apical nitrate oxygen distance to the metal center is longer [2.2731(9) Å] than the basal nitrate oxygen [1.9548(8) Å], which represents the shortest donor−acceptor distance of all. Distorted square pyramidal geometry is reflected by the angles N2−Cu1−N5 [157.61(4)°], N4−Cu1−O1 [174.59(4)°], and N4−Cu1−O4 [100.10(4)°], which deviate from ideal geometry. The acidic hydrogen atom could be located from the difference map as it forms a hydrogen bond to a nitrate oxygen atom of the neighboring complex molecule [H3···O5 1.879(9) Å].

The two complexes [Ni^{II}(PIPYH)$_2$](NO$_3$)$_2$ (**2**) (Figure 5) and [Zn^{II}(PIPYH)$_2$](NO$_3$)$_2$ (**3**) are isostructural. The metal atom is coordinated by two tridentate PIPYH ligands, leading to a distorted octahedral geometry. In general, all metal−ligand bonds are slightly shorter for the nickel complex **2** than for the zinc complex **3** due to the smaller ionic radius. All metal−ligand bond distances are in a similar range from 2.0027(17) to 2.1177(17) Å for **2** and 2.0992(11) to 2.1533(11) Å for **3**, which is in agreement with literature reported data.[35−37] Distorted octahedral geometry is evidenced by deviation of all the involved angles from ideal geometries [e.g., N2−M−N5 is 154.30(6)° for **2** and 147.44(4)° for **3**, or N2−M−N7 is 96.58(9)° for **2** and 94.30(4)° for **3**]. All acidic hydrogen atoms could be located and were found to form hydrogen bonds to the nitrate counterions.

For the cobalt complex [Co^{III}(PIPY)$_2$](NO$_3$) (**7**), two complex molecules were found in the asymmetric unit, showing only small deviations in their octahedral geometries. A representative molecule is shown in Figure 6. The metal atom is coordinated by two ligand molecules in a *mer*-tridentate fashion, forming an octahedral cation. The nitrate counterion is not coordinated. Metal−nitrogen bond lengths range from 1.875(8) to 1.948(7) Å and are significantly shorter than for complexes **1**−**3** due to the decreased ionic radius as well as the increased electrophilicity of Co^{III} with respect to Co^{II}. All bond distances match well with reported values for Co^{III}−N and are significantly shorter than expected values for the case of the divalent state.[34] The bond lengths were found to be shortest for the metal−imino nitrogen atoms N4 and N9 and the longest for the metal−pyridine nitrogen atoms N5 and N10. The same trend was also found for compounds **2** and **3**.

Acid−Base Behavior. The reactivity of nickel complex [Ni^{II}(PIPYH)$_2$](NO$_3$)$_2$ (**2**) toward bases and of [Ni^{II}(PIPYH)(PIPY)](NO$_3$) (**5**) toward acids was investigated by UV/vis spectroscopy. To a sample of the respective compound in dry acetonitrile was added up to 100 equiv of the base or acid. After the addition of 5 equiv of base or acid, respectively, a UV/vis spectrum was recorded. Surprisingly, compound **2** seems to be unreactive toward deprotonation, as the spectrum did not show significant changes after addition of either triethylamine or sodium hydroxide. Only a slight hypsochromic shift is apparent,

dx.doi.org/10.1021/ic200279g |*Inorg. Chem.* 2011, 50, 7478–7488

Table 3. Crystallographic Data and Structure Refinement for Complexes 1-3 and 7

	1	2·EtOH	3·EtOH	7·1.5EtOH
empirical formula	$CuC_{10}H_8ClN_7O_6$	$NiC_{24}H_{32}Cl_2N_{12}O_7$	$ZnC_{22}H_{22}Cl_2N_{12}O_7$	$CoC_{23}H_{23}Cl_2N_{11}O_{4.5}$
M_r, g/mol	421.22	730.23	702.79	655.35
crystal description	green column	orange column	yellow cube	black block
crystal system	monoclinic	monoclinic	triclinic	triclinic
space group	$P2(1)/n$	$C2/c$	$P\bar{1}$	$P\bar{1}$
a, Å	8.2730(3)	19.3589(17)	9.1327(5)	8.9527(8)
b, Å	14.7159(5)	10.2495(9)	10.8382(5)	15.3964(13)
c, Å	12.5797(4)	14.6535(14)	14.6431(7)	20.5716(18)
α, deg	90.00	90.00	98.457(2)	80.312(5)
β, deg	104.5530(10)	103.300(4)	90.961(3)	84.071(5)
γ, deg	90.00	90.00	97.988(2)	83.546(5)
volume, Å^3	1482.37(9)	2829.5(4)	1418.71(12)	2767.1(4)
Z	4	4	2	4
T, K	100(2)	100(2)	100(2)	100(2)
D_c, g/cm^3	1.887	1.714	1.645	1.573
μ(MoK$_\alpha$), mm^{-1}	1.703	0.945	1.120	0.868
F(000)	844	1512	716	1340
reflections collected	116698	36659	127860	26117
unique reflns	4752	4784	8988	12155
reflns with $I \geq 2\sigma(I)$	4460	4159	8327	6186
R(int), $R(\sigma)$	0.0355, 0.0116	0.0351, 0.0245	0.0326, 0.0144	0.0677, 0.1514
no. of param/restraints	226/0	186/0	399/0	703/31
final R1 [a], wR2 [b] ($I \geq 2\sigma$)	0.0214, 0.0580	0.0327, 0.0820	0.0294, 0.0761	0.0890, 0.2207
R indices (all data)	0.0237, 0.0593	0.0399, 0.0854	0.0330, 0.0788	0.1328, 0.2496
GOF on F^2	1.099	1.074	1.070	0.950
largest diff. peak and hole, e/Å^3	0.554, −0.393	0.691, −0.629	1.035, −0.613	1.512, −1.594
CCDC deposition no.	810789	810788	810790	810791

[a] $R1 = \Sigma||F_o| - |F_c||/\Sigma|F_o|$. [b] $wR2 = \{\Sigma[w(F_o^2 - F_c^2)^2]^2/\Sigma[w(F_o^2)^2\}^{1/2}$.

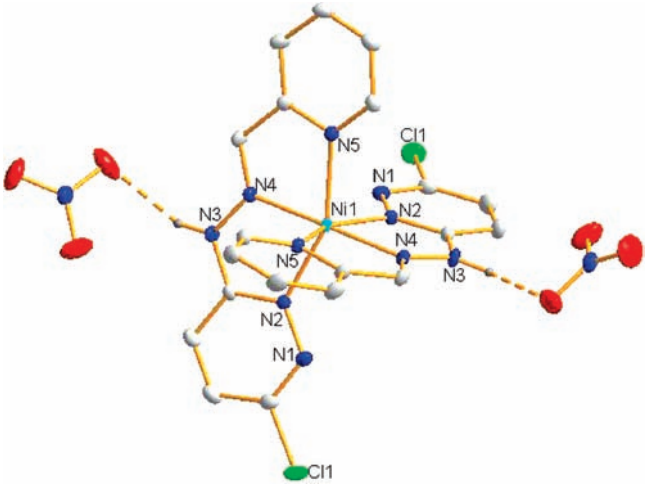

Figure 5. Molecular view of complex $[Ni^{II}(PIPYH)_2](NO_3)_2$ (**2**) (50% probability). Hydrogen atoms (except the hydrazone proton in the ligand backbone) and solvent molecules have been omitted for clarity. Hydrogen bonding is indicated by a dashed bond.

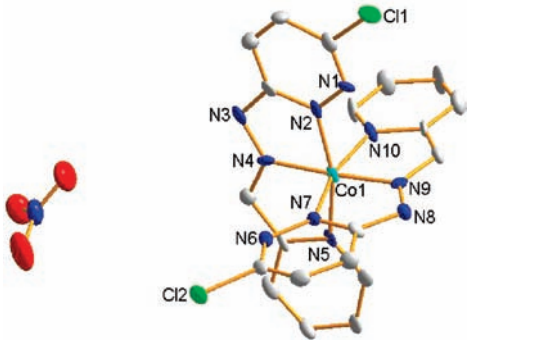

Figure 6. Molecular view of complex $[Co^{III}(PIPY)_2](NO_3)$ (**7**) (50% probability). Hydrogen atoms have been omitted for clarity. Only one molecule of the asymmetric unit is displayed.

due to altered solvent properties, but the intensities of the peaks remain unchanged. It is not clear why compound **5** can easily be obtained in situ but not by a stepwise procedure from isolated **2** and subsequent addition of base. However, compound **5** can be protonated by weak acids. Figure 7 displays UV/vis spectra of the reaction of **5** with acetic acid (100 equiv). Comparison with the spectrum of isolated **2** (inset, Figure 7) shows the course of the protonation process; however, a huge excess is required to achieve full conversion. Unfortunately, stronger acids led to decomposition of the compound, as indicated by the appearance of absorptions in the UV/vis spectrum characteristic for the uncoordinated PIPYH ligand and the disappearance of the absorptions shown in Figure 7. Analogous PAPY complexes, however, are extraordinarily stable toward strong acids or bases

dx.doi.org/10.1021/ic200279g |*Inorg. Chem.* 2011, 50, 7478–7488

and can be de- and reprotonated reversibly, rendering them suitable titration indicator substances.[28,29]

Similar protonation and proton abstraction experiments could not be performed with the two copper complexes [Cu^{II}(PIPYH)$(NO_3)_2$] (**1**) and [Cu^{II}(PIPY)(NO_3)] (**4**) due to the fact that in solution several species seem to be present, as observed by ESI-MS.

As expected, similar experiments with the Co^{III} complex **7** showed it to be unreactive toward protonation. Weak acids such as acetic acid did not affect the UV/vis spectrum, whereas strong acids like nitric acid, *p*-toluenesulfonic acid, or hydrochloric acid led to full decomposition of the compound. These observations propose a decreased coordination capability of the ligand upon introduction of an additional nitrogen atom in the heterocycle so that protonation of the backbone starts competing with displacement of the ligand.

Electrochemical Studies. Redox properties of complexes **1**, **2**, **4**, **5**, and **7** were investigated by cyclic voltammetry in dry acetonitrile solution, and the data are summarized in Table 4. Copper complexes **1** and **4** show one pseudoreversible redox couple each, with cathodic reductions at −0.920 and −0.875 V, respectively, as well as oxidative responses with narrow widths and high peak currents at −0.615 and −0.644 V, which are typical for anodic stripping of copper metal.[38] Thus, no further insight into potentially present species in solution could be obtained by CV experiments.

Nickel complexes **2** and **5** show two irreversible reduction waves with E_{pc} at −1.344 and −1.225 V, respectively, which were assigned to the redox couple $Ni^{II} \rightarrow Ni^{I}$ (Figure 8a). The negative shift of the reduction potential is caused by the ligand electron-donation ability and is similar to the potential of related nickel complexes featuring also N_6 coordination environments.[39,40] A higher electron density due to one anionic ligand is anticipated at the metal core of complex **5**, leading to a more negative reduction potential. However, the opposite trend is observed; thus the increased σ-donating ability of the deprotonated ligand is supposed to be compensated for by a significant π-acceptor contribution.

Cobalt complex **7** (Figure 8b) exhibits two reversible redox waves, which are assigned to the consecutive $Co^{III} \rightarrow Co^{II}$ ($E_{1/2}$ −0.866 V) and $Co^{II} \rightarrow Co^{I}$ ($E_{1/2}$ −1.602 V) redox processes, giving ample evidence for **7** being a Co^{III} complex.

EPR Spectroscopy and Calculations of Complexes 1 and 4. The EPR spectra obtained from powders of [Cu^{II}(PIPYH)$(NO_3)_2$] (**1**) and [Cu^{II}(PIPY)(NO_3)] (**4**) were well distinguishable but barely resolved. Since an unambiguous parameter set for the simulation of the experimental spectra was hardly attainable, we decided to perform quantum-mechanical calculations at appropriate levels of theory to determine the geometries of the complexes and, on the basis of these data, we evaluated the EPR parameters (**g** and hyperfine tensors). From the calculated EPR data, the EPR spectra were calculated and compared to the experimental counterparts.

The basis of our calculations was the X-ray geometry of [Cu^{II}(PIPYH)$(NO_3)_2$] (**1**), which we have chosen as the starting point of the computations. The initial, experimentally determined geometry was optimized by density functional theory (DFT) at the B3LYP/TZVP level of theory. The calculated geometry essentially resembles the arrangement of the ligands

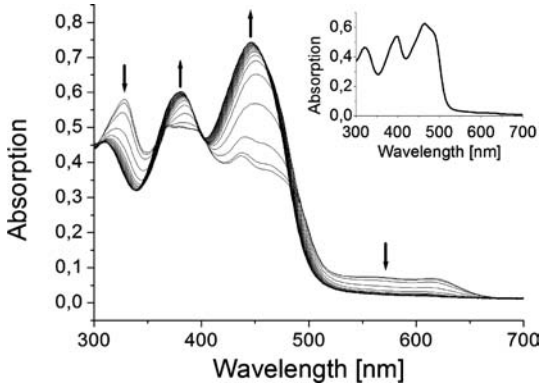

Figure 7. UV/vis spectra of the titration of **5** with 100 equiv of acetic acid in dry acetonitrile (5 equiv per spectrum). (Inset) Spectrum of isolated **2** in dry acetonitrile.

Table 4. Electrochemical Data for 1, 2, 4, 5, and 7 in Dry Acetonitrile Solution at Room Temperature[a]

compd	E_{pc}, V	E_{pa}, V	ΔE_p, mV	$E_{1/2}$, V	redox process
1	−0.920	−0.615	305	−0.768	$Cu^{II} \rightarrow Cu$
4	−0.875	−0.644	231	−0.760	$Cu^{II} \rightarrow Cu$
2	−1.365				$Ni^{II} \rightarrow Ni^{I}$
5	−1.203				$Ni^{II} \rightarrow Ni^{I}$
7	−0.902	−0.830	72	−0.866	$Co^{III} \rightarrow Co^{II}$
	−1.643	−1.561	82	−1.602	$Co^{II} \rightarrow Co^{I}$

[a] Measured by CV in CH_3CN at 50 mV/s. *E* vs $Ag/AgNO_3$. Conditions: Pt disk (working) and [$Ag^+/AgNO_3$ 0.01 M in CH_3CN, 0.1 M [nBu_4N][PF_6]] (reference) electrodes, supporting electrolyte 0.05 M TBAP solution in CH_3CN in an Ar atmosphere.

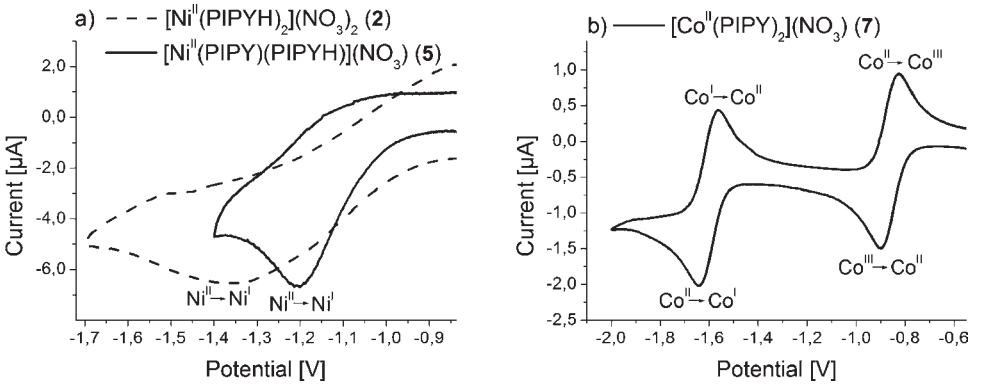

Figure 8. Cyclic voltammogram of complexes **2**, **5**, and **7** in acetonitrile solution. Scan rate 50 mV/s.

dx.doi.org/10.1021/ic200279g |*Inorg. Chem.* 2011, 50, 7478–7488

Table 5. Calculated and Experimental g and A Tensors of 1 and 4

	g_{xx}	g_{yy}	g_{zz}	A_{xx}	A_{yy}	A_{zz}
1 (calc/calc geom)[a]	2.008	2.159	2.200	32.8	164.0	405.3
1 (calc/exp geom.)[a]	2.044	2.066	2.156	13.5	92.2	536.4
1 (exp)	2.069	2.112	2.164			
4 (calc geom)[b]	2.042	2.055	2.151	18.8	22.2	538.3
4 (exp)	1.992	1.992	2.318			

[a] The EPR parameters were calculated on the basis of the computationally optimized geometry (first line) and the X-ray data (second line) of **1**. [b] No X-ray structure available.

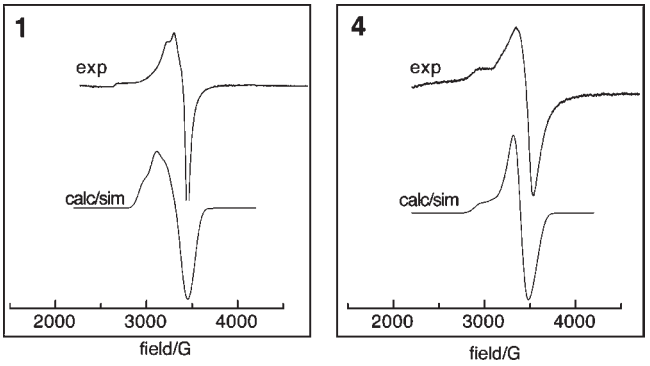

Figure 9. EPR spectra of **1** and **4** and their simulated counterparts. The simulations are accomplished with the use of calculated data presented in Table 5.

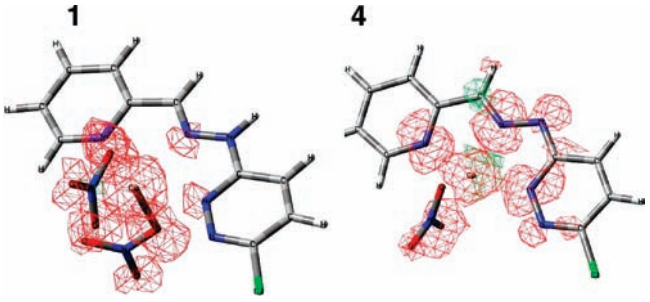

Figure 10. Spin density distributions in **1** and **4** computed at B3LYP/TZVP level (± 0.0008 au isosurfaces; positive spin density is indicated in red, negative in green).

established by X-ray structure analysis. Remarkably, however, the distances between the Cu^{II} center and the adjacent ligand N atoms are markedly longer in the calculation (see Supporting Information) than those determined by experiment. This can be explained by the experimentally observed hydrogen bonding between the (acidic) N*H* group of the PIPYH ligand and adjacent NO_3^- counterions (Figure 4). The EPR spectrum of **1** possesses no marked parallel features and a rather broad signal in the perpendicular domain. The signal could point either to distorted axial symmetry with a substantially broadened parallel region or to a substantially lower symmetry. Some more insight is provided by the calculation. It suggests a clearly nonaxial **g** and **A** tensor. The EPR parameters were calculated, on the basis of both computationally optimized geometry and, for **1**, also X-ray data. The computed EPR parameters (Table 5) based on the experimentally and computationally determined geometry display common features, leading to a reasonable fit with the experimental EPR spectrum. Using these data for the simulation of the EPR spectrum indicates a reasonable agreement with its experimental counterparts.

The N*H* proton of the PIPYH ligand and one NO_3^- anion were removed from **1** and subsequently this complex, $[Cu^{II}(PIPY)(NO_3)]$ (**4**) was optimized as described above.

The calculated **g** and **A** tensor components of **4** reflect an essentially axial symmetry. With $g_\perp = 2.048$ $[(g_{xx} + g_{yy})/2]$ and $g_\parallel = 2.151$ together with the hyperfine parameters $A_\perp$ and $A_\parallel$ = 20.5 and 538 MHz, respectively, a nicely matching simulation of the experimental EPR spectrum can be accomplished (Figure 9).

Electron Distributions in 1 and 4. The isosurface plots of the spin density distributions in **1** and **4** were computed at the same level of theory. Calculations show that, in the case of **1**, the spin population is localized mainly on the metal center and nitrate ions. Only a very low portion of the spin is present on the nitrogen atoms coordinated directly to the Cu^{II} center. Presumably the "real" spin distribution leaves a higher portion of the negative charge within the π system of the PIPYH ligand, owing to the attenuation of the charge density at the NO_3^- groups, which is caused by intermolecular hydrogen bonding (see above and Figure 4). On the other hand, in the deprotonated complex **4** the spin is distributed more uniformly between Cu^{II}, the NO_3^- counterion, and the nitrogen atoms of the PIPY ligand (Figure 10).

CONCLUSIONS

Two series of protonated and deprotonated complexes of Ni^{II}, Cu^{II}, and Zn^{II} have been synthesized and characterized by NMR, attenuated total reflection infrared (ATR-IR) and UV/vis and mass spectroscopy as well as cyclic voltammetry. Two stoichiometries were observed for the protonated complexes by X-ray crystallography, namely, ligand:metal = 1:1 for copper (**1**) and 2:1 for nickel (**2**) and zinc (**3**). The identical stoichiometries for the deprotonated counterparts in the case of copper (**4**), nickel (**5**), and zinc (**6**) were strongly indicated by EI-MS measurements. The same metal-induced preference for equimolar coordination was previously described for the $PAPYH/PAPY^-$ system.[21,32]

The semideprotonated nickel complex **5** could irreversibly be fully protonated by weak acids. ESI-MS evidenced intact complexes in solution; thus the enhanced proton affinity is tentatively ascribed to an increased π-backbonding of the ligand, which increases significantly the electron density on the ligand. These observations were supported by reduction potentials of complexes **2** and **5** obtained by CV. The ligand itself is readily deprotonated by triethylamine during complex synthesis. With the $PAPHY/PAPY^-$ system, no π-backbonding is reported. Coordination of the latter leads solely to σ-donation to the metal, which significantly increases the acidity of the abstractable hydrazone proton. The copper complexes **1** and **4** appeared to be unstable in solution as evidenced by ESI-MS; thus comparative studies could not be carried out.

For cobalt, only one type of fully deprotonated complex could be obtained, which shows a diamagnetic Co^{III} core. In the literature, the same behavior was described for the $PAPYH/PAPY^-$ system.[21,32] Co^{II} is presumably oxidized by the proton of the acidic ligand, which is reduced to H_2. This is supported by the fact that the same product is obtained in the absence of oxygen.

dx.doi.org/10.1021/ic200279g |*Inorg. Chem.* 2011, 50, 7478–7488

During complex synthesis, the acidity of the proton in the backbone is further increased by the enhanced electron density on the oxidized metal and it is lost easily. Thus, no reprotonation is feasible, as with weak acids no reaction is observed, but strong acids lead to immediate decomposition of the compound.

In the case of Cu^{II} complex **1** and its deprotonated derivative **4**, EPR spectroscopy and DFT calculations reveal a rather increased symmetry upon deprotonation. This becomes evident from the transition of the nonaxial **g** tensor for **1** to an essentially axial one for **4** and is in line with the presence of only one tightly bound NO_3^- counterion. With the decreased number of ligands, the overall symmetry is enlarged. This observation corresponds to the elimination of hydrogen bonding between the ligand and neighboring NO_3^- counterions that is present in $[Cu^{II}(PIPYH)(NO_3)_2]$ (**1**) (Figure 4).

EXPERIMENTAL SECTION

General. All chemicals were purchased from commercial sources and used without further purification.

Spectroscopy. All NMR spectra were measured on a Bruker Avance III spectrometer (300 MHz for ^{1}H and 75 MHz for ^{13}C NMR). The ^{1}H NMR spectroscopic data are reported as s = singlet, d = doublet, t = triplet, m = multiplet or unresolved, br = broad signal, coupling constant(s) in hertz, shifts in parts per million (ppm) relative to the solvent residual peak. UV titrations were performed on a Varian Cary 50 spectrophotometer with a thermostated cuvette cavity. Infrared spectra were measured on a Bruker ALPHA-P Diamant ATR-FTIR spectrometer. Mass analysis was performed on an Agilent Technologies 5975C inert XL MSD direct insertion probe spectrometer applying electron impact ionization.

EPR spectra were taken on a MS300 (Magnettech, Berlin, Germany) or Bruker EMX (Bruker, Rheinstetten, Germany) spectrometer. The samples were kept at 77 K in a dewar finger filled with liquid nitrogen (the spectra were taken at a modulation amplitude of 5 G). EPR spectra were simulated with Simfonia (Bruker, Rheinstetten, Germany).

Synthesis of 3-Hydrazino-6-chloropyridazine.[33] A solution of 3,6-dichloropyridazine (2.0 g, 13.4 mmol) in water/NH_3 (50 mL) was heated to reflux when hydrazine hydrate (4.3 g of a 25% solution, 21.5 mmol) was added. Heating was maintained for 3 h, after which full conversion was evidenced by thin-layer chromatography (TLC). After the solution was cooled to room temperature, the volume was reduced to one-third. Upon cooling the solution in an ice bath, the product precipitated as a beige crystalline material, which was filtered off and dried in vacuo to afford the product. (1.65 g, 85.2%). ^{1}H NMR (300 MHz, CD_3CN, 300 K) δ = 4.11 (br s, 3H, NH-N*H*$_2$), 7.12 (d, J = 9.3 Hz, 1H, Ar*H*$_{Pdz}$), 7.29 (d, J = 9.3 Hz, 1H, Ar*H*$_{Pdz}$), 7.50 (br s, 1H, N*H*-NH$_2$). ^{13}C NMR (75 MHz, $CDCl_3$, 300 K) δ = 116.6, 129.2, 145.9, 162.2 (aromatic carbons).

Synthesis of PIPYH. An ethanolic solution (60 mL) of 3-hydrazino-6-chloropyridazine (1.00 g, 6.9 mmol) and 1.1 equiv of 2-pyridinealdehyde (0.73 mL, 7.6 mmol) in the presence of acetic acid (3 drops) as a catalyst was heated to reflux for 45 min. After the mixture was cooled to room temperature, the precipitated product was filtered off as white needles and dried in vacuo to yield 1.21 g (75.1%) of PIPYH. ^{1}H NMR (300 MHz, CD_3CN, 300 K) δ = 11.97 (s, 1H, N*H*), 8.57 (d, J = 4.9 Hz, 1H, Ar*H*$_{Py}$), 8.16 (s, 1H, *H*N=C), 8.03 (d, J = 7.9 Hz, 1H, Ar*H*$_{Py}$), 7.83 (t, J = 7.7 Hz, 1H, Ar*H*$_{Py}$), 7.76 (d, J = 9.4 Hz, 1H, Ar*H*$_{Pdz}$), 7.71 (d, J = 9.4 Hz, 1H, Ar*H*$_{Pdz}$), 7.35 (dd, J = 7.1, 4.9 Hz, 1H, Ar*H*$_{Py}$). ^{13}C NMR (75 MHz, DMSO-d_6, 300 K) δ = 116.6, 119.8, 124.0, 130.6, 137.1, 142.8, 148.4, 149.8, 154.0, 159.2. EI-MS (m/z) 233 $[M]^+$. IR (ATR, cm^{-1}) ν = 1576 (m), 1529 (m), 1461 (m), 1407 (s), 1284 (m), 1070 (s), 830 (s), 769 (s), 713 (s), 426 (s).

General Procedure A (Synthesis of Complexes 1−3). To a boiling solution of PIPYH in ethanol was added 1 equiv of the metal salt $[Ni(NO_3)_2\cdot 6H_2O$, $Cu(NO_3)_2\cdot 3H_2O$, or $Zn(NO_3)_2\cdot 4H_2O]$ as a 0.1 M solution in ethanol. A color change was immediately apparent. The reaction mixtures were heated to reflux for an additional 20 min, followed by cooling to room temperature. The products crystallized overnight at ambient temperature by slow evaporation of the solvent. The obtained crystals were isolated by filtration and dried in vacuo.

*Synthesis of $[Cu^{II}(PIPYH)(NO_3)_2]$ (**1**).* General procedure A was followed by employing PIPYH (50 mg, 0.21 mmol) and $Cu(NO_3)_2\cdot 3H_2O$ (0.21 mmol, 2.1 mL of a 0.1 M solution in ethanol) in 10 mL of ethanol; compound **1** was obtained as green parallelepipeds (45 mg, 51%) by crystallization at room temperature overnight. IR (ATR, cm^{-1}) ν = 1594 (w), 1486 (m), 1283 (s), 1010 (m), 930 (m), 778 (s), 417 (s). EI-MS (m/z) 295 $[M - 2NO_3 - H]^+$. Anal. Calcd for $CuC_{10}H_8N_7O_6Cl$ (Found): C, 28.52 (28.77); H, 1.91 (1.59); N, 23.28 (23.15).

*Synthesis of $[Ni^{II}(PIPYH)_2](NO_3)_2$ (**2**).* General procedure A was followed by employing PIPYH (50 mg, 0.21 mmol) and $Ni(NO_3)_2\cdot 6H_2O$ (0.21 mmol, 2.1 mL of a 0.1 M solution in ethanol) in 10 mL of ethanol; compound **2** was obtained as orange rectangular rods (49 mg, 72% based on ligand) by crystallization at room temperature overnight. IR (ATR, cm^{-1}) ν = 1594 (m), 1420 (s), 1136 (s), 897 (s), 839 (s), 770 (s), 640 (s), 571 (s), 418 (m). MS (ESI in CH_3CN, m/z) 525 $[M - H]^+$. Anal. Calcd for $NiC_{20}H_{16}N_{12}O_6Cl_2\cdot H_2O$ (Found): C, 35.96 (35.89); H, 2.72 (2.56); N, 25.16 (25.41).

*Synthesis of $[Zn^{II}(PIPYH)_2](NO_3)_2$ (**3**).* General procedure A was followed by employing PIPYH (50 mg, 0.21 mmol) and $Zn(NO_3)_2\cdot 4H_2O$ (0.21 mmol, 2.1 mL of a 0.1 M solution in ethanol) in 10 mL of ethanol; compound **3** was obtained as yellow cubes (54 mg, 78% based on ligand) by crystallization at room temperature overnight. IR (ATR, cm^{-1}) ν = 1595 (m), 1424 (s), 1585 (s), 1147 (s), 782 (m), 414 (m). EI-MS (m/z) 530 $[M - 2H]^+$. Anal. Calcd for $ZnC_{20}H_{16}N_{12}O_6Cl_2\cdot 0.4(EtOH)\cdot 2H_2O$ (Found): C, 35.13 (35.13); H, 3.21 (3.20); N, 23.65 (23.62).

General Procedure B (Synthesis of Complexes 4−7). To a boiling solution of PIPYH in ethanol was added triethylamine, and the mixture was refluxed for 5 min. Subsequently 1 equiv of the metal salt $[Co(NO_3)_2\cdot 6H_2O$, $Ni(NO_3)_2\cdot 6H_2O$, $Cu(NO_3)_2\cdot 3H_2O$, or $Zn(NO_3)_2\cdot 4H_2O]$ was added as a 0.1 M solution in ethanol. An intensive color change was immediately apparent. The reaction mixtures were heated to reflux for an additional 20 min, followed by cooling to room temperature. The products crystallized overnight at ambient temperature by slow evaporation of the solvent or were precipitated by layering with diethyl ether. The obtained materials were isolated by filtration or centrifugation and dried in vacuo.

*Synthesis of $[Cu^{II}(PIPY)(NO_3)]$ (**4**).* General procedure B was followed by employing PIPYH (50 mg, 0.21 mmol), triethylamine (30 μL, 0.21 mmol), and $Cu(NO_3)_2\cdot 3H_2O$ (0.21 mmol, 2.1 mL of a 0.1 M solution in ethanol) in 10 mL of ethanol; compound **4** was obtained as dark brown microcrystalline material (29 mg, 39%) by slow evaporation of the solvent overnight. The material was washed with chloroform and dried in vacuo. IR (ATR, cm^{-1}) ν = 1600 (m), 1434 (s), 1397 (s), 1284 (s), 1097 (m), 740 (s), 674 (s), 414 (s). MS (EI, m/z) 295 $[M - NO_3]^+$. Anal. Calcd for $CuC_{10}H_7N_6O_3Cl$ (Found): C, 31.93 (32.26); H, 2.41 (2.71); N, 22.43 (21.53).

*Synthesis of $[NiII(PIPY)(PIPYH)](NO_3)$ (**5**).* General procedure B was followed by employing PIPYH (50 mg, 0.21 mmol), triethylamine (30 μL, 0.21 mmol), and $Ni(NO_3)_2\cdot 6H_2O$ (0.21 mmol, 2.1 mL of a 0.1 M solution in ethanol) in 10 mL of ethanol; compound **5** was obtained as dark brown microcrystalline material (31 mg, 50% based on ligand) by slow evaporation of the solvent overnight. The material was washed with chloroform and dried in vacuo. IR (ATR, cm^{-1}) ν = 1597 (m), 1401 (s), 1290 (s), 1124 (s), 1033 (m), 746 (m), 653 (m). MS (ESI in CH_3CN, m/z) 525 $[M]^+$. Anal. Calcd for $NiC_{20}H_{15}N_{11}Cl_2O_3\cdot CHCl_3$ (Found): C, 35.71 (35.69); H, 2.28 (2.22); N, 21.81 (22.01).

dx.doi.org/10.1021/ic200279g |*Inorg. Chem.* 2011, 50, 7478–7488

*Synthesis of [$Zn^{II}(PIPY)_2$] (**6**).* General procedure B was followed by employing PIPYH (50 mg, 0.21 mmol), triethylamine (30 μL, 0.21 mmol), and $Zn(NO_3)_2 \cdot 4H_2O$ (0.21 mmol, 2.1 mL of a 0.1 M solution in ethanol) in 10 mL of ethanol; compound **6** was obtained as an orange waxy solid (35 mg, 63% based on the ligand) by slow evaporation of the solvent. ^{1}H NMR (300 MHz, CD_3CN, 300 K) δ = 8.29 (s, 1H, *H*N=C), 7.93 (d, J = 4.6 Hz, 1H, ArH_{Py}), 7.82 (t, J = 7.7 Hz, 1H, ArH_{Py}), 7.46 (d, J = 7.7 Hz, 1H, ArH_{Py}), 7.17 (t, J = 5.0 Hz, 1H, ArH_{Py}), 7.13 (d, J = 9.5 Hz, 1H, ArH_{Pdz}), 7.07 (d, J = 9.4 Hz, 1H, ArH_{Pdz}). IR (ATR, cm^{-1}) ν = 904 (w), 1018 (w), 1097 (m), 1119 (s), 1294 (m), 1324 (s), 1398 (s), 1593 (m). EI-MS (m/z) 530 $[M]^+$. Anal. Calcd for $ZnC_{20}H_{14}N_{10}Cl_2 \cdot 1.5H_2O$ (Found): C, 43.23 (43.11); H, 3.08 (2.99); N, 25.21 (25.41).

*Synthesis of [$Co^{III}(PIPY)_2$](NO_3) (**7**).* General procedure B was followed by employing PIPYH (50 mg, 0.21 mmol), triethylamine (30 μL, 0.21 mmol), and $Co(NO_3)_2 \cdot 6H_2O$ (0.21 mmol, 2.1 mL of a 0.1 M solution in ethanol) in 10 mL of ethanol; compound **7** was obtained as a dark brown microcrystalline material (44 mg, 71% based on the ligand) after removal of the solvent. Recrystallization from ethanol gave green crystals of X-ray quality. ^{1}H NMR (300 MHz, CD_3CN, 300 K) δ = 8.88 (s, 1H, *H*N=C), 8.04 (t, J = 7.7 Hz, 1H, ArH_{Py}), 7.93 (d, J = 4.9 Hz, 1H, ArH_{Py}), 7.85 (d, J = 7.7 Hz, 1H, ArH_{Py}), 7.40 (d, J = 9.4 Hz, 1H, ArH_{Pdz}), 7.36 (m, 1H, ArH_{Pd}), 7.30 (d, J = 9.4 Hz, 1H, ArH_{Pdz}). IR (ATR, cm^{-1}) ν = 1539 (m), 1397 (s), 1323 (s), 1119 (s), 1039 (s), 747 (m), 680 (m). MS (ESI in CH_3CN, m/z) 523 $[M]^+$. Anal. Calcd for $CoC_{20}H_{14}N_{11}Cl_2O_3 \cdot 2H_2O$, brown material (Found): C, 38.60 (39.01); H, 2.92 (2.95); N, 24.76 (24.15). Calcd for $CoC_{20}H_{14}N_{11}Cl_2O_3 \cdot 0.5(EtOH) \cdot 2H_2O$, green crystals (Found): C, 40.21 (39.88); H, 3.05 (2.81); N, 24.56 (24.29).

X-ray Crystallographic Studies. Intensity data sets for compounds **1**−**3** and **7** were collected by use of a Bruker Smart APEX II diffractometer equipped with a graphite monochromator (Mo Kα radiation, λ = 0.710 73 Å) and a charge-coupled device (CCD) detector. All compounds were measured at 100 K. The structures were solved by direct methods (SHELXS-97)[41] and refined by full-matrix least-squares techniques against F^2 (SHELXL-97).[41] The asymmetric units of complexes **1**−**3** and **7** contain two metal complex molecules and those of **2** and **3** contain additionally one molecule of ethanol, and 1.5 molecules of ethanol were found in **7**. In the latter, one anion was found to be disordered over two sites, which were refined with site occupation factors fixed at 0.5. For the disordered NO_3^- anion, the displacement parameters of the N atom were constrained to be the same and the six N−O distances were restrained to the same value. Two ill-defined ethanol molecules could not be refined properly; thus the electron density was removed from the data set with the PLATON SQUEEZE routine[42] and modeled as one fully occupied and one-half occupied ethanol molecule per metal center. All non-hydrogen atoms were refined with anisotropic displacement parameters without any constraints. Data were corrected for absorption and *Lp* factors with SADABS.[43] Hydrogen atoms were placed geometrically and refined by use of a riding model.

Electrochemical Methods. Redox chemical properties of complexes **1**, **2**, **4**, and **7** were carried out in an argon-filled glovebox by use of a Gamry Reference 600 potentiostat connected to a personal computer. Cyclic voltammograms were obtained in 0.05 M solution $[nBu_4N][PF_6]/CH_3CN$ at 25 °C. The experiments were carried out in a three-electrode glass cell with a platinum disk (d = 3 mm) working electrode, a platinum wire auxiliary electrode, and a $[Ag^+/AgNO_3$ 0.01 M in CH_3CN, 0.1 M $[nBu_4N][PF_6]]$ reference electrode. Under these conditions, oxidation of ferrocene occurs at 0.095 V.

Protonation Studies. UV/vis spectra were measured on a Varian Cary 50 spectrophotometer equipped with a thermostated cuvette holder (25 °C). In a typical experiment, 2 mL of a 0.025 mM solution of the complex was placed in the photometer. One milliliter of a 2.5 mM solution of the reagent was added in 10 portions of 100 μL each, which correspond to 10 equiv. After each addition, a spectrum was acquired. All spectra were corrected for dilution by applying the Lambert−Beer law on the supposition that ε remains constant.

Computational Details. The geometries of $[Cu^{II}(PIPYH)(NO_3)_2]$ (**1**) and $[Cu^{II}(PIPY)(NO_3)]$ (**4**) complexes used for the hyperfine structure and **g**-tensor computations were optimized in unrestricted Kohn−Sham calculations at the B3LYP[44−46] level by use of the Turbomole[47] package. The basis sets were of polarized triple-ζ quality for all atoms (TZVP).[48] All hyperfine calculations were carried out with the ORCA[49] program package at the optimized geometries and with the hybrid B3LYP functional. The choice of this functional was based on previous computations, which show that it is very successful in the prediction of hyperfine coupling (HFC) and **g**-tensor in nitrogen and Cu^{II} complexes.[50−53] Ligand atoms were treated by Huzinaga−Kutzelnigg type basis sets BII (denoted also as IGLO-II).[54,55] For Cu center, an accurate triply polarized basis set CP(PPP) was employed.[52] This basis set is especially flexible in the core region and is believed to provide results close to the basis set limit for the Fermi contact interaction. Because the spin−orbit effects are known to influence the HFC results for 3d transition metal complexes, in the case of the copper atom the contributions of spin−orbit coupling (SOC) to the HFC were taken into account. It was proven that implementation of SOC contributions into the HFC computations results in significant improvement of calculated parameters when compared to experiment.[53,56] The calculation of **g**-tensor values was carried out with the same geometry and basis sets. A common gauge at the copper atom was employed. ORCA package was used also for generating the isosurface plots of spin density distributions at the B3LYP/TZVP level.

■ ASSOCIATED CONTENT

Supporting Information. Three figures showing molecular view of complex **3** and Mulliken atomic spin densities for complexes **1** and **4**. This material is available free of charge via the Internet at http://pubs.acs.org. X-ray crystallographic data for **1**, **2**, **3** and **7** are also available (CCDC reference numbers 810789, 810788, 810790, and 810791).

■ AUTHOR INFORMATION

Corresponding Author
*E-mail: nadia.moesch@uni-graz.at.

■ ACKNOWLEDGMENT

We acknowledge fForte−Wissenschafterinnenkolleg FreChe Materie for financial support. We are grateful to Dr. Christine Onitsch for help with the EPR spectra.

■ REFERENCES

(1) Zoller, G.; Strobel, H.; Will, D. W.; Wohlfart, P. PCT Int. Appl. WO 2008 104279 A1, 2008.
(2) Durand-Reville, T.; Jewell, C.; Hammond, C.; Chin, D. PCT Int. Appl. WO 2008 030579, 2008.
(3) Watterson, D. M.; van Eldik, L.; Haiech, J.; Hibert, M.; Bourguignon, J.-J.; Velentza, A.; Hu, W.; Zasadzki, M. PCT Int. Appl. WO 2006 050359, 2006.
(4) Trah, S.; Lamberth, C.; Wendeborn, S. V. PCT Int. Appl. WO 2009 090039, 2009.
(5) Lamberth, C.; Wendeborn, S. V.; Trah, S.; Dumeunier, R. PCT Int. Appl. WO 2008 089934, 2008.
(6) Grote, T.; Gypser, A.; Rheinheimer, J.; Rose, I.; Schaefer, P.; Schieweck, F.; Sauter, H.; Gewehr, M.; Mueller, B.; Tormo i Blasco, J.; Ammermann, E.; Strathmann, S.; Lorenz, G.; Stierl, R. PCT Int. Appl. WO 2002 074753 A3, 2002.

(7) Deng, Z.; Tseng, H.-W.; Zong, R.; Wang, D.; Thummel, R. P. *Inorg. Chem.* **2008**, *47*, 1835–1848.
(8) Price, J. R.; Lan, Y.; Brooker, S. *Dalton Trans.* **2007**, 1807–1820.
(9) Ohno, K.; Arima, K.; Tanaka, S.; Yamagata, T.; Tsurugi, H.; Mashima, K. *Organometallics* **2009**, *28*, 3256–3263.
(10) Manzano, B. R.; Jalon, F. A.; Ortiz, I. M.; Soriano, M. L.; La Gomez Torre, F.; de; Elguero, J.; Maestro, M. A.; Mereiter, K.; Claridge, T. D. W. *Inorg. Chem.* **2008**, *47*, 413–428.
(11) Thompson, L. K.; Woon, T. C.; Murphy, D. B.; Gabe, E. J.; Lee, F. L.; Le Page, Y. *Inorg. Chem.* **1985**, *24*, 4719–4725.
(12) Escuer, A.; Vicente, R.; Mernari, B.; El Gueddi, A.; Pierrot, M. *Inorg. Chem.* **1997**, *36*, 2511–2516.
(13) Brooker, S. *Eur. J. Inorg. Chem.* **2002**, 2535–2547.
(14) Beckmann, U.; Brooker, S. *Coord. Chem. Rev.* **2003**, *245*, 17–29.
(15) Allan, J. R.; Barnes, G. A.; Brown, D. H. *J. Inorg. Nucl. Chem.* **1971**, *33*, 3765–3771.
(16) An, C. X.; Li, X. R.; Zhang, Z. H. *Transition Met. Chem.* **2009**, *34*, 255–261.
(17) Seleem, H. S. *J. Indian Chem. Soc.* **2003**, *80*, 622–625.
(18) Blake, A. J.; Hubberstey, P.; Li, W.-S.; E.Russell, C.; Smith, B. J.; Wraith, L. D. *Inorg. Chem.* **1998**, *4*, 647–656.
(19) Mahmoud, F. Z.; Ramadan, A. A. T.; Ali, D. A. *J. Coord. Chem.* **2008**, *61*, 2639–2654.
(20) Grünwald, K. R.; Saischek, G.; Volpe, M.; Belaj, F.; Mösch-Zanetti, N. C. *Eur. J. Inorg. Chem.* **2010**, *15*, 2297–2305.
(21) Lions, F.; Martin, K. V. *J. Am. Chem. Soc.* **1957**, *80*, 3858–3865.
(22) Green, R. W.; Hallman, P. S.; Lions, F. *Inorg. Chem.* **1963**, *3*, 376–381.
(23) Chiswell, B.; Geldard, J. F.; Phillip, A. T.; Lions, F. *Inorg. Chem.* **1964**, *3*, 1272–1277.
(24) Mesa, J. L.; Arriortua, M. I.; Lezama, L.; Pizarro, J. L.; Rojo, T.; Beltran, D. *Polyhedron* **1988**, *7*, 1383–1388.
(25) Rojo, T.; Mesa, J. L.; Arriortua, M. I.; Savariault, J. M.; Galy, J.; Villeneuve, G.; Beltran, D. *Inorg. Chem.* **1988**, *27*, 3904–3911.
(26) Gerloch, M. *J. Chem. Soc. A* **1966**, 1317–1325.
(27) Geldard, J. F.; Lions, F. *Inorg. Chem.* **1963**, *2*, 270–282.
(28) Bell, C. F.; Quddus, M. A. *Anal. Chim. Acta* **1970**, *52*, 313–321.
(29) Cameron, A. J.; Gibson, N. A. *Anal. Chim. Acta* **1970**, *51*, 249–256.
(30) Quddus, M. A.; Bell, C. F. *J. Inorg. Nucl. Chem.* **1971**, *33*, 2001–2007.
(31) Quddus, M. A.; Bell, C. F. *Anal. Chim. Acta* **1968**, *42*, 503–513.
(32) Heit, M. L.; Ryan, D. E. *Anal. Chim. Acta* **1965**, *32*, 448–455.
(33) Farina, C.; Pinza, M.; Cerri, A.; Parravinci, F. PCT Int. Appl. EP 274409 A2, 1988.
(34) Kime, N. E.; Ibers, J. A. *Acta Crystallogr.* **1969**, *B25*, 168–169.
(35) Otieno, T.; Rettig, S. J.; Thompson, R. C.; Trotter, J. *Inorg. Chem.* **1995**, *34*, 1718–1725.
(36) Dumitru, F.; Petit, E.; van der Lee, A.; Barboiu, M. *Eur. J. Inorg. Chem.* **2005**, 4255–4262.
(37) Dumitru, F.; Legrand, Y.-M.; Barboiu, M.; Petit, E.; van der Lee, A. *Cryst. Growth Des.* **2009**, *9*, 2917–2921.
(38) Sarkar, B.; Konar, S.; Gomez-Garcia, C. J.; Ghosh, A. *Inorg. Chem.* **2008**, *47*, 11611–11619.
(39) Prasad, K. T.; Scaife, D. B. *J. Electroanal. Chem.* **1977**, *84*, 373–386.
(40) Brodovitch, J. C.; Haines, R. I.; McAuley, A. *Can. J. Chem.* **1981**, *59*, 1610–1614.
(41) Sheldrick, G. M. *Acta Crystallogr.* **2008**, *A64*, 112–122.
(42) van der Sluis, P.; Spek, A. L. *Acta Crystallogr.* **1990**, *A 46*, 194–201.
(43) *SADABS*, v2008-1; Bruker AXS, 2008.
(44) Becke, A. D. *Phys. Rev. A* **1988**, *38*, 3098–3100.
(45) Becke, A. D. *J. Chem. Phys.* **1993**, *98*, 1372–1377.
(46) Becke, A. D. *J. Chem. Phys.* **1993**, *98*, 5648–5652.
(47) Ahlrichs, R.; Bar, M.; Haser, M.; Horn, H.; Kölmel, C. *Chem. Phys. Lett.* **1989**, *162*, 165–169.
(48) Schäfer, A.; Huber, C.; Ahlrichs, R. *J. Chem. Phys.* **1994**, *100*, 5829–5835.
(49) Neese, F. *ORCA, an ab initio, density functional and semiempirical program package*, University of Bonn, Germany, 2007
(50) Neese, F. *J. Phys. Chem. A* **2001**, *105*, 4290–4299.
(51) Kaupp, M.; Reviakine, R.; Malkina, O. L.; Arbuznikov, A.; Schimmelpfennig, B.; Malkin, V. G. *J. Comput. Chem.* **2002**, *23*, 794–803.
(52) Neese, F. *Inorg. Chim. Acta* **2002**, *337*, 181–192.
(53) Remenyi, C.; Reviakine, R.; Arbuznikov, A. V.; Vaara, J.; Kaupp, M. *J. Phys. Chem.* **2004**, *108*, 5026–5033.
(54) Kutzelnigg, W.; Schindler, M.; Fleischer, U. In *Deuterium and Shift Calculations*; Diehl, P., Fluck, E., Günther, H., Kosfeld, R., Seelig, J., Eds.; NMR Basic Principles and Progress, Vol. 23; Springer: Berlin and Heidelberg, Germany, 1990
(55) Huzinaga, S. *Approximate Atomic Functions*, University of Alberta, Canada, 1971
(56) Neese, F. *J. Chem. Phys.* **2003**, *118*, 3939–3948.